Biomedical Optics EXPRESS

Photoacoustic and ultrasound imaging using dual contrast perfluorocarbon nanodroplets triggered by laser pulses at 1064 nm

Alexander S. Hannah,[1] Donald VanderLaan,[1,2] Yun-Sheng Chen,[1,2] and Stanislav Y. Emelianov[1,2,*]

[1]*The Department of Biomedical Engineering, The University of Texas at Austin, Austin, TX 78712, USA*
[2]*The Department of Electrical and Computer Engineering, The University of Texas at Austin, Austin, TX 78712, USA*
[*]*emelian@mail.utexas.edu*

Abstract: Recently, a dual photoacoustic and ultrasound contrast agent—named photoacoustic nanodroplet—has been introduced. Photoacoustic nanodroplets consist of a perfluorocarbon core, surfactant shell, and encapsulated photoabsorber. Upon pulsed laser irradiation the perfluorocarbon converts to gas, inducing a photoacoustic signal from vaporization and subsequent ultrasound contrast from the resulting gas microbubbles. In this work we synthesize nanodroplets which encapsulate gold nanorods with a peak absorption near 1064 nm. Such nanodroplets are optimal for extended photoacoustic imaging depth and contrast, safety and system cost. We characterized the nanodroplets for optical absorption, image contrast and vaporization threshold. We then imaged the particles in an *ex vivo* porcine tissue sample, reporting contrast enhancement in a biological environment. These 1064 nm triggerable photoacoustic nanodroplets are a robust biomedical tool to enhance image contrast at clinically relevant depths.

OCIS codes: (110.5120) Photoacoustic imaging; (170.7170) Ultrasound; (160.4236) Nanomaterials; (170.3880) Medical and biological imaging; (170.7180) Ultrasound diagnostics.

References and links

1. C. G. A. Hoelen, F. F. M. de Mul, R. Pongers, and A. Dekker, "Three-dimensional photoacoustic imaging of blood vessels in tissue," Opt. Lett. **23**(8), 648–650 (1998).
2. M. Xu and L. V. Wang, "Photoacoustic imaging in biomedicine," Rev. Sci. Instrum. **77**(4), 041101 (2006).
3. J. J. Niederhauser, M. Jaeger, R. Lemor, P. Weber, and M. Frenz, "Combined ultrasound and optoacoustic system for real-time high-contrast vascular imaging in vivo," IEEE Trans. Med. Imaging **24**(4), 436–440 (2005).
4. S. Sethuraman, S. R. Aglyamov, J. H. Amirian, R. W. Smalling, and S. Y. Emelianov, "Intravascular photoacoustic imaging using an IVUS imaging catheter," IEEE Trans. Ultrason. Ferroelectr. Freq. Control **54**(5), 978–986 (2007).
5. S. Sethuraman, J. H. Amirian, S. H. Litovsky, R. W. Smalling, and S. Y. Emelianov, "Spectroscopic intravascular photoacoustic imaging to differentiate atherosclerotic plaques," Opt. Express **16**(5), 3362–3367 (2008).
6. A. Pope-Harman, M. M.-C. Cheng, F. Robertson, J. Sakamoto, and M. Ferrari, "Biomedical Nanotechnology for Cancer," Med. Clin. North Am. **91**(5), 899–927 (2007).
7. P. Sharma, S. Brown, G. Walter, S. Santra, and B. Moudgil, "Nanoparticles for bioimaging," Adv. Colloid Interface Sci. **123-126**, 471–485 (2006).
8. J. N. Anker, W. P. Hall, O. Lyandres, N. C. Shah, J. Zhao, and R. P. Van Duyne, "Biosensing with plasmonic nanosensors," Nat. Mater. **7**(6), 442–453 (2008).
9. G. P. Luke, D. Yeager, and S. Y. Emelianov, "Biomedical Applications of Photoacoustic Imaging with Exogenous Contrast Agents," Ann. Biomed. Eng. **40**(2), 422–437 (2012).
10. J. L. Bo Wang, J. L. Su, A. B. Karpiouk, K. V. Sokolov, R. W. Smalling, and S. Y. Emelianov, "Intravascular photoacoustic imaging," IEEE J. Sel. Top. Quantum Electron. **16**(3), 588–599 (2010).
11. S. Y. Nam, L. M. Ricles, L. J. Suggs, and S. Y. Emelianov, "In vivo ultrasound and photoacoustic monitoring of mesenchymal stem cells labeled with gold nanotracers," PLoS ONE **7**(5), e37267 (2012).

#216307 - $15.00 USD Received 7 Jul 2014; revised 11 Aug 2014; accepted 12 Aug 2014; published 14 Aug 2014

12. D.-A. Clevert, K. Stock, B. Klein, J. Slotta-Huspenina, L. Prantl, U. Heemann, and M. Reiser, "Evaluation of Acoustic Radiation Force Impulse (ARFI) imaging and contrast-enhanced ultrasound in renal tumors of unknown etiology in comparison to histological findings," Clin. Hemorheol. Microcirc. **43**(1-2), 95–107 (2009).
13. R. Lencioni, D. Cioni, and C. Bartolozzi, "Tissue harmonic and contrast-specific imaging: back to gray scale in ultrasound," Eur. Radiol. **12**(1), 151–165 (2002).
14. E. G. Schutt, D. H. Klein, R. M. Mattrey, and J. G. Riess, "Injectable Microbubbles as Contrast Agents for Diagnostic Ultrasound Imaging: The Key Role of Perfluorochemicals," Angew. Chem. Int. Ed. Engl. **42**(28), 3218–3235 (2003).
15. J. R. Lindner, J. Song, F. Xu, A. L. Klibanov, K. Singbartl, K. Ley, and S. Kaul, "Noninvasive Ultrasound Imaging of Inflammation Using Microbubbles Targeted to Activated Leukocytes," Circulation **102**(22), 2745–2750 (2000).
16. D. B. Ellegala, H. Leong-Poi, J. E. Carpenter, A. L. Klibanov, S. Kaul, M. E. Shaffrey, J. Sklenar, and J. R. Lindner, "Imaging Tumor Angiogenesis With Contrast Ultrasound and Microbubbles Targeted to αvβ3," Circulation **108**(3), 336–341 (2003).
17. A. Agarwal, S. W. Huang, M. O'Donnell, K. C. Day, M. Day, N. Kotov, and S. Ashkenazi, "Targeted gold nanorod contrast agent for prostate cancer detection by photoacoustic imaging," J. Appl. Phys. **102**(6), 064701 (2007).
18. G. Kim, S.-W. Huang, K. C. Day, M. O'Donnell, R. R. Agayan, M. A. Day, R. Kopelman, and S. Ashkenazi, "Indocyanine-green-embedded PEBBLEs as a contrast agent for photoacoustic imaging," J. Biomed. Opt. **12**(4), 044020 (2007).
19. L. Tong, Q. Wei, A. Wei, and J.-X. Cheng, "Gold Nanorods as Contrast Agents for Biological Imaging: Optical Properties, Surface Conjugation and Photothermal Effects," Photochem. Photobiol. **85**(1), 21–32 (2009).
20. K. Wilson, K. Homan, and S. Emelianov, "Biomedical photoacoustics beyond thermal expansion using triggered nanodroplet vaporization for contrast-enhanced imaging," Nat. Commun. **3**, 618 (2012).
21. E. Strohm, M. Rui, I. Gorelikov, N. Matsuura, and M. Kolios, "Vaporization of perfluorocarbon droplets using optical irradiation," Biomed. Opt. Express **2**(6), 1432–1442 (2011).
22. A. Hannah, G. Luke, K. Wilson, K. Homan, and S. Emelianov, "Indocyanine Green-Loaded Photoacoustic Nanodroplets: Dual Contrast Nanoconstructs for Enhanced Photoacoustic and Ultrasound Imaging," ACS Nano **8**(1), 250–259 (2014).
23. C. W. Wei, M. Lombardo, K. Larson-Smith, I. Pelivanov, C. Perez, J. Xia, T. Matula, D. Pozzo, and M. O'Donnell, "Nonlinear contrast enhancement in photoacoustic molecular imaging with gold nanosphere encapsulated nanoemulsions," Appl. Phys. Lett. **104**(3), 033701 (2014).
24. C. W. Wei, J. Xia, M. Lombardo, C. Perez, B. Arnal, K. Larson-Smith, I. Pelivanov, T. Matula, L. Pozzo, and M. O'Donnell, "Laser-induced cavitation in nanoemulsion with gold nanospheres for blood clot disruption: in vitro results," Opt. Lett. **39**(9), 2599–2602 (2014).
25. N. Rapoport, K.-H. Nam, R. Gupta, Z. Gao, P. Mohan, A. Payne, N. Todd, X. Liu, T. Kim, J. Shea, C. Scaife, D. L. Parker, E.-K. Jeong, and A. M. Kennedy, "Ultrasound-mediated tumor imaging and nanotherapy using drug loaded, block copolymer stabilized perfluorocarbon nanoemulsions," J. Control. Release **153**(1), 4–15 (2011).
26. N. Y. Rapoport, A. M. Kennedy, J. E. Shea, C. L. Scaife, and K.-H. Nam, "Controlled and targeted tumor chemotherapy by ultrasound-activated nanoemulsions/microbubbles," J. Control. Release **138**(3), 268–276 (2009).
27. M. M. Kaneda, S. Caruthers, G. M. Lanza, and S. A. Wickline, "Perfluorocarbon Nanoemulsions for Quantitative Molecular Imaging and Targeted Therapeutics," Ann. Biomed. Eng. **37**(10), 1922–1933 (2009).
28. N. Rapoport, Z. Gao, and A. Kennedy, "Multifunctional Nanoparticles for Combining Ultrasonic Tumor Imaging and Targeted Chemotherapy," J. Natl. Cancer Inst. **99**(14), 1095–1106 (2007).
29. C. J. Murphy, A. M. Gole, J. W. Stone, P. N. Sisco, A. M. Alkilany, E. C. Goldsmith, and S. C. Baxter, "Gold Nanoparticles in Biology: Beyond Toxicity to Cellular Imaging," Acc. Chem. Res. **41**(12), 1721–1730 (2008).
30. T. Niidome, M. Yamagata, Y. Okamoto, Y. Akiyama, H. Takahashi, T. Kawano, Y. Katayama, and Y. Niidome, "PEG-modified gold nanorods with a stealth character for in vivo applications," J. Control. Release **114**(3), 343–347 (2006).
31. S.-S. Yu, S.-S. Chang, C.-L. Lee, and C. R. C. Wang, "Gold nanorods: electrochemical synthesis and optical properties," J. Phys. Chem. B **101**(34), 6661–6664 (1997).
32. S. Link, M. B. Mohamed, and M. A. El-Sayed, "Simulation of the Optical Absorption Spectra of Gold Nanorods as a Function of Their Aspect Ratio and the Effect of the Medium Dielectric Constant," J. Phys. Chem. B **103**(16), 3073–3077 (1999).
33. R. G. M. Kolkman, E. Hondebrink, W. Steenbergen, and F. F. M. de Mul, "In vivo photoacoustic imaging of blood vessels using an extreme-narrow aperture sensor," IEEE J. Sel. Top. Quantum Electron. **9**(2), 343–346 (2003).
34. K. Homan, S. Kim, Y.-S. Chen, B. Wang, S. Mallidi, and S. Emelianov, "Prospects of molecular photoacoustic imaging at 1064 nm wavelength," Opt. Lett. **35**(15), 2663–2665 (2010).
35. P. K. Jain, K. S. Lee, I. H. El-Sayed, and M. A. El-Sayed, "Calculated Absorption and Scattering Properties of Gold Nanoparticles of Different Size, Shape, and Composition: Applications in Biological Imaging and Biomedicine," J. Phys. Chem. B **110**(14), 7238–7248 (2006).
36. J. Yang, T. Ling, W.-T. Wu, H. Liu, M.-R. Gao, C. Ling, L. Li, and X.-W. Du, "A top-down strategy towards monodisperse colloidal lead sulphide quantum dots," Nat. Commun. **4**, 1695 (2013).

#216307 - $15.00 USD Received 7 Jul 2014; revised 11 Aug 2014; accepted 12 Aug 2014; published 14 Aug 2014

37. I. Radko, M. G. Nielsen, O. Albrektsen, and S. I. Bozhevolnyi, "Stimulated emission of surface plasmon polaritons by lead-sulphide quantum dots at near infra-red wavelengths," Opt. Express **18**(18), 18633–18641 (2010).
38. I. Gorelikov, A. L. Martin, M. Seo, and N. Matsuura, "Silica-Coated Quantum Dots for Optical Evaluation of Perfluorocarbon Droplet Interactions with Cells," Langmuir **27**(24), 15024–15033 (2011).
39. Y.-S. Chen, W. Frey, S. Aglyamov, and S. Emelianov, "Environment-Dependent Generation of Photoacoustic Waves from Plasmonic Nanoparticles," Small **8**(1), 47–52 (2012).
40. Y. Du, X. H. Hu, M. Cariveau, X. Ma, G. W. Kalmus, and J. Q. Lu, "Optical properties of porcine skin dermis between 900 nm and 1500 nm," Phys. Med. Biol. **46**(1), 167–181 (2001).
41. J. L. Prince and J. Links, *Medical Imaging Signals and Systems*, 1st ed. (Prentice Hall, 2005).
42. A. Oppelt, *Imaging Systems for Medical Diagnostics: Fundamentals, Technical Solutions and Applications for Systems Applying Ionizing Radiation, Nuclear Magnetic Resonance and Ultrasound* (John Wiley & Sons, 2011).
43. A. Webb and G. C. Kagadis, "Introduction to Biomedical Imaging," Med. Phys. **30**(8), 2267 (2003).
44. O. D. Kripfgans, J. B. Fowlkes, D. L. Miller, O. P. Eldevik, and P. L. Carson, "Acoustic droplet vaporization for therapeutic and diagnostic applications," Ultrasound Med. Biol. **26**(7), 1177–1189 (2000).
45. T. O. Matsunaga, P. S. Sheeran, S. Luois, J. E. Streeter, L. B. Mullin, B. Banerjee, and P. A. Dayton, "Phase-Change Nanoparticles Using Highly Volatile Perfluorocarbons: Toward a Platform for Extravascular Ultrasound Imaging," Theranostics **2**(12), 1185–1198 (2012).
46. N. Reznik, R. Williams, and P. N. Burns, "Investigation of Vaporized Submicron Perfluorocarbon Droplets as an Ultrasound Contrast Agent," Ultrasound Med. Biol. **37**(8), 1271–1279 (2011).
47. P. S. Sheeran, S. H. Luois, L. B. Mullin, T. O. Matsunaga, and P. A. Dayton, "Design of ultrasonically-activatable nanoparticles using low boiling point perfluorocarbons," Biomaterials **33**(11), 3262–3269 (2012).
48. N. Rapoport and K. H. Nam, "Droplet-To-Bubble Transition in Phase-Shift Nanoemulsions for Tumor Chemotherapy," Int. J. Transp. Phenom. **12**, 51–62 (2011).
49. American National Standards Institute and Laser Institute of America, *American National Standard for Safe Use of Lasers* (Laser Institute of America, 2007).
50. R. Asami and K. Kawabata, "Repeatable vaporization of optically vaporizable perfluorocarbon droplets for photoacoustic contrast enhanced imaging," in *Ultrasonics Symposium (IUS), 2012 IEEE International* (2012), pp. 1200–1203.

1. Introduction

Photoacoustic (PA) imaging is an emerging diagnostic technique capable of high resolution, real-time, depth-resolved visualization of tissue [1,2]. The contrast in PA imaging arises from differential optical absorption, where deep-seated absorbers are detected through photoacoustic (i.e., high-frequency pressure or ultrasound) transient waves. Photoacoustics can be synergistically integrated with ultrasound (US) given that the two systems can share components responsible for detecting sound waves [3–5].

Endogenous contrast in PA imaging is limited to differences in optical absorption among biological chromophores, which may not be sufficient for the detection and characterization of a disease such as cancer or atherosclerosis [6–11]. Furthermore, contrast in pulse-echo US imaging arises from differences in acoustic impedance, which is also often inadequate for early diagnosis of tumors and other pathological processes [12,13]. Consequently, various formulations of injectable particles or solutions have been developed to locally amplify signal. Ultrasound utilizes gas microbubbles [14–16], which provide acoustic impedance mismatch to surrounding tissue, whereas PA contrast agents—such as dyes and nanoparticles—rely on their high optical absorption relative to biological tissue [9,17–19].

More recently, optically-triggered liquid perfluorocarbon (PFC) nanodroplets have been used to improve contrast for both ultrasound and photoacoustic imaging as well as therapeutic purposes [20–24]. These photoacoustic nanodroplets (PAnDs) comprise a liquid PFC core with an encapsulated photoabsorber, all surrounded by a stabilizing surfactant shell. Upon pulsed laser irradiation, the nanodroplets undergo vaporization – a process that provides a strong PA signal and, therefore, local enhancement of contrast. Furthermore, the resulting microbubbles backscatter sound waves, providing enhanced contrast in conventional pulse-echo ultrasound.

Unlike larger gas bubbles used for US contrast enhancement, liquid nanodroplets exhibit a half-life *in vivo* of several hours [25], and they have the ability to escape vascular compartments and penetrate deeper into tissue [26]. In addition, surface modification allows for active particle targeting of tumor cells [27]. Once in a superheated state in the body and

#216307 - $15.00 USD Received 7 Jul 2014; revised 11 Aug 2014; accepted 12 Aug 2014; published 14 Aug 2014

accumulated at a site of interest, a low-energy optical trigger can locally vaporize the droplets, providing a mechanism for remotely triggered activation. Incorporation of therapeutics render the droplets externally activated drug delivery vehicles [28]. The limitations of PAnDs are that they require an optical trigger of sufficient fluence to induce activation, and the PA contrast from vaporization only occurs instantaneously upon droplet vaporization for droplets made of low boiling point PFCs, whereas sustainable PA signal requires a stable, higher boiling point PFC droplet. Previously, PAnDs with encapsulated gold nanorods have been imaged *in vivo* using light with wavelength of 780 nm [20]. To further advance this technology, we exploit several properties of gold nanorods, including their biocompatibility [29,30], high optical absorption [31], well-known chemistry for surface modification [17], and especially their tunability to absorb at specific wavelengths [32]. Biomedical imaging with light at 1064 nm improves contrast due to minimal absorption by blood-perfused tissue at this wavelength [33], and imaging can be performed with an inexpensive single wavelength Nd:YAG laser source [34], so extension of PAnDs to activation at 1064 nm is a natural progression of the technology. Minimal absorption of 1064 nm light results in higher local fluence deeper into tissue, requiring lower incident laser fluence and encapsulation of fewer gold nanoparticles. While other formulations of PAnDs made with lead sulfide particles are triggered with 1064 nm light [21], gold nanoparticles are stronger optical absorbers, which would increase vaporization sensitivity [35–37]. In addition, PA and US image contrast enhancement using optically triggered nanodroplets in a biological environment at 1064 nm has not yet been reported.

In this work, we synthesize high aspect ratio gold nanorods, characterize their optical absorption, and incorporate them into PAnDs. We then perform imaging experiments to quantify the changes in contrast and contrast-to-noise ratio (CNR) upon irradiation of PAnDs by a pulsed Nd:YAG laser emitting light at 1064 nm. Furthermore, we measure the laser fluence threshold necessary to induce PAnD vaporization detectable by diagnostic US imaging. Lastly, we conduct US and PA imaging on PAnDs injected into porcine tissue *ex vivo*, and we report the image contrast enhancement in an environment closely mimicking clinical conditions.

2. Methods

2.1. Synthesis of photoacoustic nanodroplets

High aspect ratio gold nanorods were produced using a seed-mediated growth method in an acidic condition. The growth solution was made by adding 5.2 mL $AgNO_3$ (4 mM), 44 mL of water, 19.2 mL of HCl (1 M), and 8 mL of $HAuCl_4$ (10 mM) to 80 mL of CTAB (0.20 M) under gentle mixing, followed by the addition of 2.4 mL of ascorbic acid (0.0788 M). To make the seed solution, in a separate vial, 2.5 mL of CTAB solution (0.20 M) was mixed with 1.5 mL of $HAuCl_4$ solution (1 mM). Then 0.60 mL of ice-cold $NaBH_4$ solution (10 mM) was added to the mixture and vigorously stirred for 2 min at 25°C, which resulted in the formation of a brownish yellow seed solution. To grow nanorods, 0.32 mL of the seed solution was added to the growth solution at 27–30 °C under gentle stirring for 30 seconds. The solution then aged for another 12 hours at 27–30 °C. The resulting gold nanorod solution was centrifuged at 5,000 rcf for 15 min to discard unwanted gold nanosphere side products; the nanospheres were concentrated in a pellet, while the nanorods remained in suspension. To reduce CTAB concentration, the nanorods were centrifuged twice at 18,000 rcf for 45 minutes. The CTAB-stabilized gold nanorod dispersion was added to an equal volume of aqueous mPEG-thiol (0.2 mM) solution under vigorous stirring. The mixture was sonicated for 5 minutes and left to react for 8 hours. Excess mPEG-thiol molecules were removed by centrifugation filtration at 3,000 rcf for 10 min, and the PEGylated gold nanorods were re-suspended in water.

#216307 - $15.00 USD Received 7 Jul 2014; revised 11 Aug 2014; accepted 12 Aug 2014; published 14 Aug 2014

The PEGylated gold nanorods were then imaged using transmission electron microscopy shown in Fig. 1(a). The surface chemistry of the PEGylated nanorods renders them hydrophilic and thus insoluble in organic PFC, shown in Fig. 1(b). To solubilize the nanorods in PFC, the surface of the nanorods was modified using an adapted method by Gorelikov et al [38]. Briefly, 15 mL of PEGylated nanorods were added to 5 mL of methanol and centrifuged at 2,500 rcf for 15 minutes. The supernatant was discarded, and the nanorods were resuspended in 15 mL of methanol. This was repeated 4 times. To fluorinate the nanorods, 300 µL of 1H,1H,2H,2H-perfluorodecyl-triethoxysilane was added to 15 mL of nanorods in methanol and stirred for 5 minutes, followed by the addition of 5 mL of a 28% ammonium hydroxide in water solution and stirred for 24 hours. The supernatant was removed by decanting and air flow, and the nanorods were resuspended in 0.3 mL of perfluoropentane by sonication. To synthesize the PAnDs, 0.3 mL of the now PFC-soluble nanorods, shown in Fig. 1(c), was added to 2.2 mL of phosphate buffered saline (0.01 M) and 0.5 mL of 1% v/v Zonyl FSO fluorosurfactant, which was then vigorously shaken and sonicated using an ultrasonic cleaner. The solution was extruded through a 1.0 µm polycarbonate membrane in order to ensure that droplet size did not significantly exceed 1.0 µm. Previous studies of similar particles report a mean size of 600 nm diameter [22]. The extinction spectrum of the aqueous nanorods was measured, which is shown Fig. 1(d), using a spectrophotometer to confirm the peak absorption wavelength. Previous formulations of optically triggered perfluorocarbon droplets show small shifts in peak optical absorption, as well as broadening of the absorption peak during nanodroplet synthesis [20,22]. This is consistent with modeled and measured optical properties of other composite nanoconstructs such as nanorods coated with silica of various thicknesses [39]. The aqueous nanorods strongly absorb light around 1060 nm. While the nanorod-loaded PAnDs exhibit scattering that increases at lower wavelengths, the strongest absorption remains in the NIR range, allowing them to be activated by an Nd:YAG laser emitting 1064 nm light.

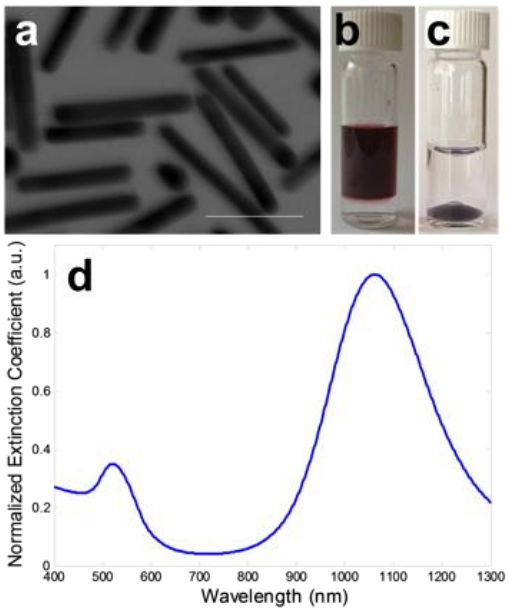

Fig. 1. Transmission electron microscope image (a) of gold nanorods. Scale bar = 50 nm. Aqueous nanorods (b) phase separated from colorless PFC. Fluorinated nanorods in PFC (c), phase separated from water. Absorption spectrum (d) of PEGylated gold nanorods.

#216307 - $15.00 USD Received 7 Jul 2014; revised 11 Aug 2014; accepted 12 Aug 2014; published 14 Aug 2014

2.2 Tissue-mimicking phantom preparation

To construct a tissue-mimicking phantom, a poly-acrylamide hydrogel was synthesized. The following components were stirred in a 125 mL Büchner flask: 64 mL DI water, 21 mL 19:1 bis-acrylamide, and 850 µL of 10% w/v ammonium persulfate. A rubber stopper was applied to the top of the flask and a vacuum tube was connected to the side. The mixture was degassed by simultaneously applying a vacuum to the flask and partially submerging it in a Branson 1510 ultrasonic cleaner in Degas mode for 5 minutes. The vacuum was removed and 50 µL of PAnDs ($3x10^{11}$ droplets/mL) were added to the mixture, while it stirred gently for 10 s. Then 106.25 µL of tetramethylethylenediamine was added to the mixture and stirred gently for another 10 s to initiate crosslinking. This mixture was poured into a 6x6x4 cm plastic box and left to polymerize at room temperature for 20 minutes. The final droplet concentration within the phantom was approximately 10^8 droplets/mL.

2.3. Phantom imaging

The phantom was brought to 37 °C in a water bath. To induce vaporization, a pulsed Nd:YAG laser was used to irradiate the phantom at a fluence of up to 90 mJ/cm^2, a value greater than the fluence threshold for droplet vaporization under these conditions. An air beam of spot size approximately 27 mm^2 directly irradiated the phantom. To demonstrate that droplet vaporization is localized to the region of irradiation, a star shaped vinyl mask was used to cover the phantom, and the phantom was mechanically scanned during irradiation, so that only the unmasked region was exposed to the laser. After irradiation, the phantom was imaged with a Vevo 2100 US imaging system. A 21 MHz array transducer was used in pulse/receive mode to collect B-mode data of the phantom, shown in Fig. 2(a). The data were processed into a 2-D image and displayed on a 50 dB logarithmic scale to exhibit the differences between the liquid nanodroplets and the vaporized bubbles.

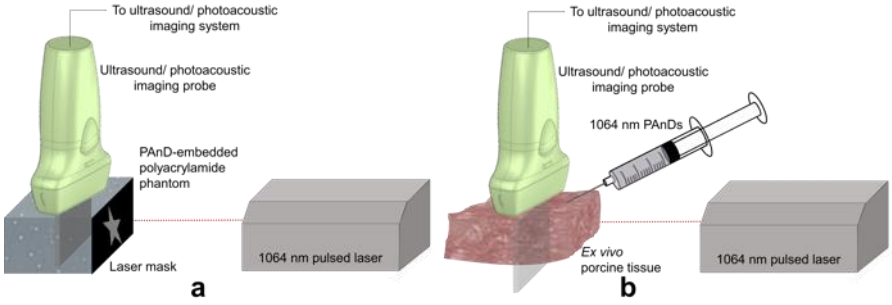

Fig. 2. Phantom imaging setup (a): tissue-mimicking polyacrylamide embedded with PAnDs and irradiated with 1064 nm pulsed laser light. *Ex vivo* imaging schematic (b): porcine tissue injected with PAnDs, then probed simultaneously using B-mode ultrasound and photoacoustic imaging techniques.

2.4. *Ex-vivo* imaging

We conducted US and 1064 nm PA imaging studies of the PAnDs in a biological environment using porcine tissue as an imaging medium, whose optical and acoustic absorption and scattering mimic human tissue [40]. A portion of the tissue, free of large pieces of fat, was cut into a 3x3x1 cm slab and brought to 37 °C in a water bath. Before injection of nanodroplets, the tissue was imaged using US and PA systems to establish background signal. Next, a 0.5 mL bolus of PAnDs (3×10^{11} droplets/mL) was injected into the sample, 1 cm from the front of the tissue where the laser is incident, and 1 cm from the top surface where the US transducer contacts the sample, using US imaging to guide a needle and to insure the injection of the droplets within the imaging plane. While the laser light was blocked, the tissue was imaged simultaneously with US and PA techniques, establishing a PA

#216307 - $15.00 USD Received 7 Jul 2014; revised 11 Aug 2014; accepted 12 Aug 2014; published 14 Aug 2014

noise floor and measuring US contrast of the injected liquid-phase PAnDs. The sample was then exposed to 1064 nm laser light pulses at a fluence of 90 mJ/cm^2 while PA and US image data was collected over 20 pulses, at a rate of 20 pulses/s.

The data was analyzed to quantify the ability to visualize the PAnDs vaporization within the porcine tissue and to measure the contribution of the particles to image signal over the native tissue. To do so, two contrast metrics were considered: the absolute contrast and local contrast. The absolute contrast, or modulation, is given as follows:

$$Contrast_{abs}\left[\frac{\mu\left(A_{i,ROI}\right)-\mu(A_{i,blank})}{\mu(A_{i,blank})}\right] \tag{1}$$

where $\mu(A_{i,ROI})$ is the mean signal amplitude of the PAnDs in the region of interest, calculated using 12 sub-sections, and $\mu(A_{i,blank})$ is the mean amplitude of an image with no target. For PA images, $\mu(A_{i,blank})$ is the mean PA image amplitude when the laser source is blocked from irradiating the target. For US images, $\mu(A_{i,blank})$ is the mean US image amplitude of a sample of degassed water.

Local contrast within the porcine tissue sample was measured as follows:

$$Contrast_{local}=\left[\frac{\mu\left(A_{i,ROI}\right)-\mu(A_{i,tissue})}{\mu(A_{i,tissue})}\right] \tag{2}$$

where $\mu(A_{i,tissue})$ is the mean amplitude of the surrounding regions of the contrast-enhanced image. From these data, the contrast-to-noise ratios (CNRs) were considered. These were calculated using the following formulas:

$$CNR_{abs}=20*log_{10}\left[\frac{\mu\left(A_{i,ROI}\right)-\mu(A_{i,blank})}{\sigma(A_{i,blank})}\right] \tag{3}$$

and

$$CNR_{local}=20*log_{10}\left[\frac{\mu\left(A_{i,ROI}\right)-\mu(A_{i,tissue})}{\sigma(A_{i,tissue})}\right] \tag{4}$$

where $\sigma(A_{i,blank})$ and $\sigma(A_{i,tissue})$ are the standard deviations of the average signal amplitudes in each sub-section for images with no target and images of porcine tissue, respectively. Sectioning was used to diminish the contribution of speckle to the CNR while obtaining an adequate number of averages. Either 9 (porcine tissue) or 16 (phantom) sub-regions—based on the size of the ROI—were used to calculate CNR. Each sub-region was approximately 0.66 mm^2. These measurements are of particular interest when quantifying the ability of a contrast agent to be distinguished, especially in a biological environment [41–43].

2.5. PAnD imaging characterization

The tendency of a droplet to vaporize depends first on the total energy deposited into the particle, which is determined by local fluence [21], optical absorber concentration, and the presence of an external ultrasound field [44]. It also depends on physical parameters that govern the stability of a liquid droplet, such as droplet diameter [44,45], photoabsorber concentration [46], environmental temperature, shell stiffness [46], PFC boiling point [47], local droplet concentration [46], and viscoelasticity of the surrounding medium. While keeping all other variables constant, the laser fluence was varied in a phantom setup to determine the threshold for US visualization of PAnD vaporization. This imaging setup was constructed similar to that in Fig. 2, with two major differences: the sample was not moved

#216307 - $15.00 USD Received 7 Jul 2014; revised 11 Aug 2014; accepted 12 Aug 2014; published 14 Aug 2014

during laser irradiation and US data were collected immediately before, during and after irradiation. The concentration of droplets within the phantom was approximately 10^7 droplets/mL, decreased in this experiment to reduce US signal from nanodroplets prior to vaporization, providing a clear distinction for detecting vaporization threshold.

Image data from each sample was divided into two frames, before and after irradiation. For each of these frames, the following metrics were calculated:

$$signal\left(dB\right) = \sum_{pixels\ in\ ROI} 20 * log_{10}(A) \tag{5}$$

and

$$\Delta signal\left(dB\right) = signal_{after\ irradiation} - signal_{before\ irradiation} \tag{6}$$

where A is the linear US amplitude at a given pixel in the image. To quantify the difference in US signal after vaporization, $\Delta\ signal$ was plotted as a function of laser fluence, including 0 mJ/cm^2 (i.e., no laser irradiation) to show noise of the measurement.

3. Results

3.1. PAnD imaging characterization

Following the selectively masked irradiation of droplet-laden phantoms, the B-mode scans exhibited greater echogenicity in the irradiated regions, shown in Fig. 3. After the liquid-to-gas transition of the liquid nanodroplet into a gas microbubble, the local mechanical properties are greatly perturbed, resulting in a contrast of 33 (unitless), and a contrast-to-noise ratio (CNR) of 41 dB.

Irradiation of the phantom at increasing levels of fluence results in the vaporization of more droplets, and thus greater increases in echogenicity, which is quantified in Figs. 4(a) and 4(b) and shown visually from ultrasound images before laser irradiation in Figs. 4(c)-4(e), and after irradiation in Figs. 4(f)-4(h). This population of droplets ranges from 200 to 800 nm in diameter. At low laser fluence, only the largest droplets vaporize, because they require the least energy to undergo phase change. At higher fluence, the smaller droplets vaporize as well [46–48]. To determine the threshold for vaporization that is detectable by US in these conditions, the change in US signal was calculated at various fluence levels, and the threshold was considered to be the fluence at which a significant change in echogenicity is measured. In these conditions, a minimum fluence of 4 mJ/cm^2 was necessary to induce vaporization that results in a detectable change in US signal, shown in Fig. 4(b).

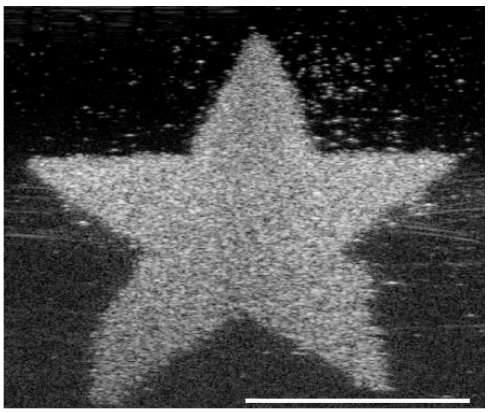

Fig. 3. Ultrasound image of a PAnD-embedded polyacrylamide phantom. A mask was used to selectively irradiate the phantom into a star shape, inducing droplet vaporization and thus increased US echogenicity in the region. Scale bar = 10 mm.

#216307 - $15.00 USD Received 7 Jul 2014; revised 11 Aug 2014; accepted 12 Aug 2014; published 14 Aug 2014

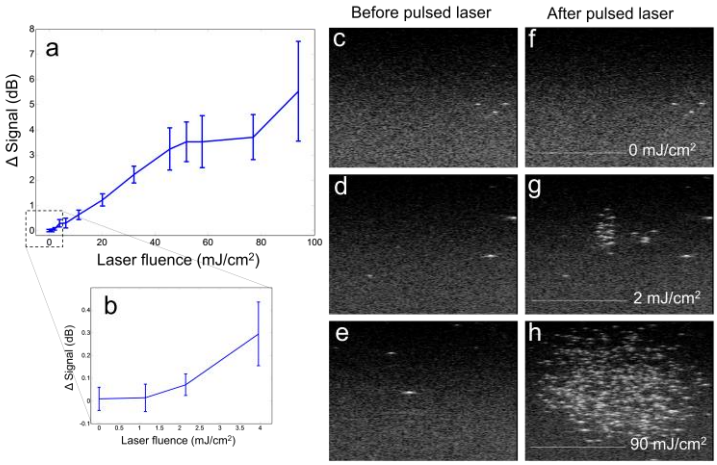

Fig. 4. Ultrasound signal difference as a function of laser fluence (a). Ultrasound signal difference at low laser fluences (b), demonstrating the fluence at which measurable vaporization is detected. Droplet-laden polyacrylamide construct before pulsed laser irradiation (c-e). Construct after irradiation at various fluences (f-h), showing droplet vaporization. Images displayed on a 50 dB scale. Scale bar = 5 mm.

*3.2. Ex vivo i*maging of PAnDs

Photoacoustic and ultrasound images of the PAnDs before and after vaporization in *ex vivo* porcine tissue are shown in Fig. 5. The highest PA signal—which is emitted as a result of droplet vaporization—occurs immediately after the application of pulsed laser light at t = 0.5 s. Subsequent PA signal results from thermal expansion of the gold nanorods and is much lower than signal from vaporization. In addition, an increase in US echogenicity persists following droplet vaporization. Quantitative measurements of contrast and CNR in the ROI are given in Table 1, which were calculated using Eqs. (5) and (6).

Ultrasound echogenicity is enhanced greatly with the activation of PAnDs into bubbles upon pulsed laser irradiation, resulting in high local contrast and CNR both in a phantom and in *ex vivo* settings. The porcine tissue exhibits little native US contrast; however, local contrast is increased 18 times in the presence of bubbles, while the CNR doubles. The tissue provides nearly zero endogenous PA signal, but the contrast and CNR increase dramatically upon vaporization of the PAnDs.

Table 1. Contrast and contrast-to-noise ratio for various samples measured with and without PAnDs.

	$Contrast_{abs}$	CNR_{abs} (dB)	$Contrast_{local}$	CNR_{local} (dB)
Ultrasound Signal				
Native porcine tissue	1.56	23	N/A	N/A
Bubbles in polyacrylamide phantom	31	44	21	37
PFC bubbles in porcine tissue	28	48	10	29
Photoacoustic Signal				
Native porcine tissue	N/A	N/A	N/A	N/A
PAnD vaporization in porcine tissue	38	50	38	50
Thermal expansion in porcine tissue	3.2	27	3.2	27

#216307 - $15.00 USD Received 7 Jul 2014; revised 11 Aug 2014; accepted 12 Aug 2014; published 14 Aug 2014

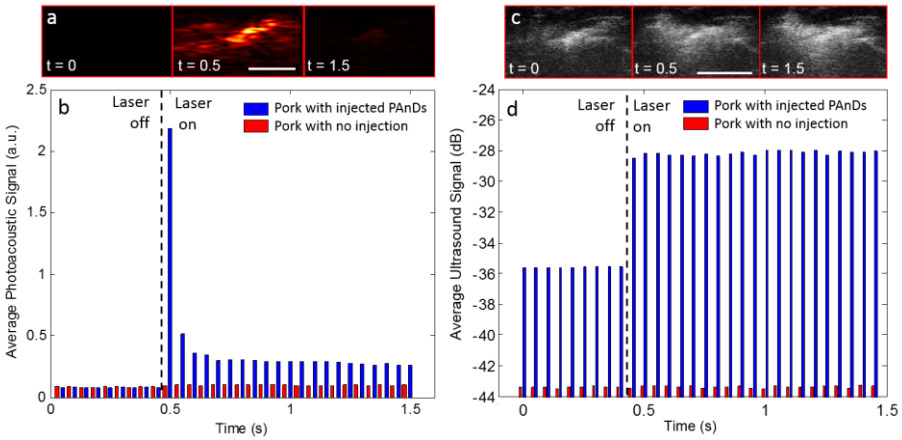

Fig. 5. Photoacoustic images of *ex vivo* porcine tissue injected with PAnDs (a), imaged before and during pulsed laser irradiation. Scale bar = 5 mm. Average PA signal over time (b) for native tissue and tissue injected with PAnDs. Ultrasound images of the same tissue sample (c) imaged before and during laser irradiation. Scale bar = 5 mm. Average US echogenicity over time (d) for PAnD injected tissue.

4. Discussion and conclusion

We have demonstrated the synthesis of a dual contrast agent which is tuned to absorb and thus be activated by 1064 nm pulsed laser light for enhanced US and PA imaging, the first agent to be made using high aspect ratio gold nanorods made soluble in PFC. Utilizing localized irradiation, the droplets may be activated at a site of interest, inducing droplet vaporization for enhanced contrast and potential release of encapsulated therapeutics.

The threshold for droplet vaporization is of interest because biological safety determines the maximum level of fluence that may be used to irradiate human subjects with pulsed NIR lasers. In these experimental conditions, the threshold is approximately 4 mJ/cm^2, well under the limit for exposure on human skin [49]. However, it is noted that the fluence required for vaporization is dependent on many factors, including photoabsorber concentration, droplet size, temperature, and elasticity of the medium. In biological media, the local fluence will be attenuated due to light scattering and absorption by tissue components. To compensate for this loss, the emitted fluence must be greater than that required locally at the target tissue depth. To mimic the optical properties of human tissue, the droplets were injected in porcine tissue and activated with pulsed laser light at a fluence of 90 mJ/cm^2. In clinical settings, the American National Standards Institute (ANSI) allows for laser fluences up to 100 mJ/cm^2 at 1064 nm when imaging through the skin [49]. It is therefore feasible that these droplets may be activated with clinically acceptable laser energy levels. In the future, we will alter parameters of the droplet formulation to render them more sensitive to vaporization, allowing for deeper imaging using lower laser fluence levels.

There are several limitations to this contrast agent. Although it has been shown that PEGylated gold nanorods are not cytotoxic *in vitro* [29,30], regulatory approval will be required before clinical translation of the PAnD construct, due to the inclusion of gold nanorods within the droplet. Furthermore, the strong PA signal from vaporization of the PAnDs is a one-time event, only after the initial pulse of light; however, other strategies have been employed to induce reversible vaporization of nanodroplets, which may be feasible for these particles in the future [50]. Lastly, upon droplet vaporization, the fate of the encapsulated nanorods is largely unknown. To utilize their PA contrast, the nanorods must be directed to actively, or passively accumulate in a tumor region.

In summary, we have developed and characterized a photoacoustic nanodroplet capable of vaporization using 1064 nm pulsed laser irradiation. Using a mask, we demonstrated localized

#216307 - $15.00 USD Received 7 Jul 2014; revised 11 Aug 2014; accepted 12 Aug 2014; published 14 Aug 2014

droplet activation at 37 °C, indicating that the droplets are stable in the body and activated only upon external trigger. We then characterized the fluence threshold for vaporization in a phantom setup, and used an *ex vivo* porcine tissue sample to demonstrate the signal and contrast enhancement of US and PA signal, which we then quantified. These nanodroplets have potential for imaging of dense tissue for tumor location using an inexpensive light source and can act as a triggered drug delivery vehicle for therapeutic purposes.

Acknowledgments

Partial support from the Breast Cancer Research Foundation and National Institutes of Health (grantsCA158598, NS082518, and EB008101) is acknowledged.

#216307 - $15.00 USD Received 7 Jul 2014; revised 11 Aug 2014; accepted 12 Aug 2014; published 14 Aug 2014